Journal of Systems Engineering and Electronics
Vol. 31, No. 6, December 2020, pp.1297 – 1307

Distributed cooperative control of autonomous multi-agent UAV systems using smooth control

BELKACEM Kada[1,*], MUNAWAR Khalid[2], and MUHAMMAD Shafique Shaikh[2]

1. Department of Aerospace Engineering, King Abdulaziz University, Jeddah 21589, Saudi Arabia;
2. Department of Electrical and Computer Engineering, King Abdulaziz University, Jeddah 21589, Saudi Arabia

Abstract: This paper addresses the cooperative control problem of multiple unmanned aerial vehicles (multi-UAV) systems. First, a new distributed consensus algorithm for second-order nonlinear multi-agent systems (MAS) is formulated under the leader-following approach. The algorithm provides smooth input signals to the agents' control channels, which avoids the chattering effect generated by the conventional sliding mode-based control protocols. Second, a new formation control scheme is developed by integrating smooth distributed consensus control protocols into the geometric pattern model to achieve three-dimensional formation tracking. The Lyapunov theory is used to prove the stability and convergence of both distributed consensus and formation controllers. The effectiveness of the proposed algorithms is demonstrated through simulation results.

Keywords: cooperative control, distributed consensus, three-dimensional formation control, multiple-UAV system.

DOI: 10.23919/JSEE.2020.000100

1. Introduction

The concept of cooperative control for multiple aerial vehicles has been developed in response to the increasing need in performing complex missions. Aerial multi-agent systems (MAS), as well as many other MAS, can perform cooperative tasks with numerous advantages such as efficiency, accuracy, flexibility, robustness, and cost-effectiveness. Multiple aircraft [1−3], helicopters [4], spacecraft [5,6], satellites [7,8], missiles [9,10], and unmanned aerial vehicles (UAV) [11−19] are among aerospace MAS.

Multi-UAV cooperative control is one of the very interesting and challenging areal MAS applications since it allows the achievement of complex missions with more flexibility, reconfiguration, adaptation to dynamic environments, and distribution. In recent years, numerous studies have tackled the problem of multi-UAV cooperative control by using different approaches and theories.

Using the contract net protocol, a task assignment model of manned/unmanned aerial vehicle formation was built in [11] to assign tasks in dynamic environments. In [12], authors formulated the formation control problem of multi-UAV systems as a differential game problem where an open-loop Nash strategy was for each agent to build a fully distributed formation control. The virtual structure approach was used in [13] to build a nonsmooth distributed cohesive motion control for the formation of autonomous quadrotor aircraft. In [14], a distributed formation flying control algorithm was developed by using a nonsmooth backstepping design approach. Adaptive formation control was developed in [15] by using a differential evolution algorithm to design the optimized formation control among a group of UAVs. The problem of formation-containment control for multiple multirotor UAV was solved in [16] by using a Riccati equation-based algorithm. In [17], a distributed self-organized mission planning algorithm was proposed for the formation control of multi-UAV systems. Voronoi diagram or partition was used in [18] to design a distributed formation control without collision. The work in [19] studied the problem of path planning within the formation control strategy using the fast particle swarm optimization where chaos-based initialization, parameter optimization, and topology update were considered to reach formation with constraints and without collisions. In [20], sliding-PID control was proposed for linear multi-agent that can be adapted for multi-UAV systems.

Although the aforementioned protocols and techniques have been shown to be effective, important issues remain to be addressed with regard to the cooperative control of MAS in general and multi-UAV systems in particular. Among these issues, one can site, control input smooth-

Manuscript received November 20, 2019.
*Corresponding author.
This work was supported by the Deanship of Scientific Research (DSR) at King Abdulaziz University, Jeddah (G-363-135-1438).

ness, switching communication topology, partial loss of communication within MAS, and formation keeping. In this paper, we address the aforementioned issues and propose solutions within a smooth distributed consensus and formation control framework. To this end, a smooth distributed consensus control is developed for multi-agent with inherent nonlinear dynamics, which is our first contribution. The control inputs to the agent closed-loop dynamics are designed by using continuous PI-like (proportional-integral) control instead of signum-based control used in the conventional discontinuous control, which results in the chattering of controllers. The second contribution of this paper is to build an aerospace formation control model. The formation model is designed by combining translational and rotational distributed protocols with a six-degree-of-freedom dynamic model in one framework.

The rest of the paper is organized as follows. The problem of distributed consensus for the second-order MAS is formulated in Section 2. In Section 3, a new distributed consensus control algorithm is developed and its stability is analyzed by using the Lyapunov-like function. In Section 4, a three-dimension formation control of autonomous aerial flying vehicles is developed via expansion of planar formation presented in [21]. Section 5 presents simulation scenarios including aerobatic consensus following and three-dimensional helicoidal formation keeping. Concluding remarks are presented in Section 6.

2. Preliminaries and problem formulation

2.1 Graph theory

Information exchange topology of a networked system of n agents can be modeled by using the graph theory. The interaction among an agent set $\mathcal{M}=\{1,2,\cdots,n\}$ is represented by a weighted graph $\mathcal{G}=(\mathcal{V},\mathcal{E},\boldsymbol{A})$ where $\mathcal{V}=(v_1, v_2,\cdots,v_n)$ denotes the vertex set, $\mathcal{E}\subseteq\mathcal{V}\times\mathcal{V}$ denotes an edge set, and $\boldsymbol{A}=(a_{ij}\geqslant 0)\in\mathbf{R}^{n\times n}$ describes a nonnegative adjacency matrix. The elements a_{ij} are defined such that $a_{ij}>0$ if $(v_i,v_j)\in\mathcal{E}$, $a_{ij}=0$ if $(v_i,v_j)\notin\mathcal{E}$, and $a_{ii}=0$ (no self-loop).

Definition 1 For each agent $i\in\mathcal{M}$, it is associated with a connectivity set $\mathcal{N}_i=\{v_i|(v_j,v_i)\in\mathcal{E}\}$ that refers to the set of the neighbors of the agent i.

Definition 2 To the graph $\mathcal{G}$, it is associated with a Laplacian matrix $\boldsymbol{L}(l_{ij})\in\mathbf{R}^{n\times n}$ such that $l_{ij}=-a_{ij}$ for $i\neq j$ and $l_{ii}=\sum_{j=1,j\neq i}^{n}a_{ij}$.

Assumption 1 The graph $\mathcal{G}$ is supposed to be connected through a direct or indirect communication topology and at least one agent follower is connected to the leader. In directed communication, the information exchange is unidirectional, while for undirected communication, the exchange of information bidirectionally results in a symmetric matrix $\boldsymbol{A}$ (due to the symmetry of the coupling weights).

Lemma 1 The Laplacian matrix $\boldsymbol{L}$ has the following key properties [22]:

(i) $\boldsymbol{L}$ is a symmetric positive semi-definite matrix ($\boldsymbol{L}=\boldsymbol{L}^T\geqslant 0$).

(ii) $\lambda_1=0$ is an eigenvalue of $\boldsymbol{L}$ with the associated eigenvector $\mathbf{1}_n=[1,1,\cdots,1]^{\mathrm{T}}$. The remaining eigenvalues of $\boldsymbol{L}$ have the positive real part with

$$0=\lambda_1(\boldsymbol{L})<\lambda_2(\boldsymbol{L})\leqslant\cdots\leqslant\lambda_n(\boldsymbol{L}).$$

(iii) $\boldsymbol{L}\mathbf{1}_n=0$.

2.2 Distributed consensus problem for nonlinear second-order MAS

Consider the case of MAS composed of one virtual leader 0 and n followers with identical nonlinear uncertain second-order dynamics

$$\begin{cases}\dot{\boldsymbol{x}}_i=\boldsymbol{v}_i\\ \dot{\boldsymbol{v}}_i=\boldsymbol{f}_i(t,\boldsymbol{x}_i,\boldsymbol{v}_i)+\boldsymbol{u}_i\end{cases}\tag{1}$$

where $\boldsymbol{x}_i,\boldsymbol{v}_i,\boldsymbol{u}_i\in\mathbf{R}^m$, denote the ith agent's position, velocity and control input vectors, respectively. The virtual leader dynamics are described as

$$\begin{cases}\dot{\boldsymbol{x}}_0=\boldsymbol{v}_0\\ \dot{\boldsymbol{v}}_0=\boldsymbol{f}_0(t,\boldsymbol{x}_0)\end{cases}\tag{2}$$

with $\boldsymbol{x}_0,\boldsymbol{v}_0\in\mathbf{R}^m$ being the leader's position and its velocity vectors. The functions $\boldsymbol{f}_0,\boldsymbol{f}_i\in\mathbf{R}^m$ represent the leader and followers dynamics, respectively.

Assumption 2 For system (1) to be stabilizable, the functions $\boldsymbol{f}_i$ are supposed to be uniformly bounded with respect to t and locally uniformly bounded with respect to $\boldsymbol{x}_i$ and $\boldsymbol{v}_i$. It results in that

$$\|\boldsymbol{f}_i(t,\boldsymbol{x}_i,\boldsymbol{v}_i)\|_2\leqslant\delta_{f_i}\tag{3}$$

where $\delta_{f_i}\in\mathbf{R}^+$.

3. Distributed consensus control algorithm

In this section, we study the problem of smooth distributed consensus control for the second-order nonlinear MAS where we consider the case of time-varying velocities. The control objective is to design distributed individual protocols $\boldsymbol{u}_i$ to achieve the following consensus agreement:

$$\begin{cases}\lim\limits_{t\to\infty}\|\boldsymbol{x}_i(t)-\boldsymbol{x}_0(t)\|_2=0\\ \lim\limits_{t\to\infty}\|\boldsymbol{v}_i(t)-\boldsymbol{v}_0(t)\|_2=0\end{cases}\quad\forall i\in\nu.\tag{4}$$

To solve this consensus problem, we propose the fol-

lowing smooth distributed control protocols:

$$\boldsymbol{u}_i(t) = -\alpha \boldsymbol{\eta}_i^{\gamma} - \beta \int_0^t \boldsymbol{\eta}_i(\tau)\mathrm{d}\tau \tag{5}$$

where

$$\boldsymbol{\eta}_i(t) = \sum_{j=0}^{n} a_{ij}(\boldsymbol{x}_i(t) - \boldsymbol{x}_j(t)) + c\sum_{j=0}^{n} a_{ij}(\boldsymbol{v}_i(t) - \boldsymbol{v}_j(t)). \tag{6}$$

The exponent γ is a positive constant that is fixed by the designer, $a_{i0} = 1$ if the agent i receives information from the leader and $a_{i0} = 0$ otherwise, α and β are control gains, and $c \in \mathbf{R}^+$.

Assumption 3 There exists a constant $\delta_L \in \mathbf{R}^+$ for which

$$\left\| \boldsymbol{L} \otimes \boldsymbol{I}_p \right\|_{\infty} \leqslant \delta_L \lambda_{max}(\boldsymbol{L}) \tag{7}$$

where $\boldsymbol{I}_p$ denotes the p-identity matrix, p=n×m.

Theorem 1 Suppose that Assumptions 1−3 hold and the communication graph $\mathcal{G}$ is connected. If the control parameters of the distributed protocols (5)−(6) satisfy

$$\begin{cases} \delta > 0 \\ \alpha > \begin{pmatrix} \gamma \\ 0 \end{pmatrix}^{-1} \dfrac{1}{\lambda_2^{\gamma+1}(\boldsymbol{L})} \left(\dfrac{2V_x(0)}{\lambda_{max}(\boldsymbol{L})} \right)^{1-\gamma} \\ \beta > \dfrac{\alpha \delta_{f_i}}{(1+c)\lambda_{max}(\boldsymbol{L} \otimes \boldsymbol{I}_p)} \end{cases}, \tag{8}$$

then the nonlinear leader-follower MAS (1)−(2) reaches the consensus argument (4). λ denotes an eigenvalue and $V_x(0) = V_x(t=0)$ denotes the Lyapunov function associated to the agents' position.

Proof For notational simplicity, we omit the time dependency. The proof is described by the following multi-step procedure.

Step 1 Define the vectors $\tilde{\boldsymbol{x}}_i = \boldsymbol{x}_i - \boldsymbol{x}_0 \in \mathbf{R}^m, \tilde{\boldsymbol{v}}_i = \boldsymbol{v}_i - \boldsymbol{v}_0 \in \mathbf{R}^m$, $\boldsymbol{\xi}_x = [\tilde{\boldsymbol{x}}_1^{\mathrm{T}}, \cdots, \tilde{\boldsymbol{x}}_n^{\mathrm{T}}]^{\mathrm{T}} \in \mathbf{R}^p$, $\boldsymbol{\xi}_v = [\tilde{\boldsymbol{v}}_1^{\mathrm{T}}, \cdots, \tilde{\boldsymbol{v}}_n^{\mathrm{T}}]^{\mathrm{T}} \in \mathbf{R}^p$ and $u = [\boldsymbol{u}_1^{\mathrm{T}}, \cdots, \boldsymbol{u}_n^{\mathrm{T}}]^{\mathrm{T}} \in \mathbf{R}^p$ ($p = n \times m$). Using those notations, the systems (1)−(2) become

$$\begin{cases} \dot{\boldsymbol{\xi}}_x = \boldsymbol{\xi}_v \\ \dot{\boldsymbol{\xi}}_v = \boldsymbol{f}(\boldsymbol{\xi}_v) + \boldsymbol{u} \end{cases}. \tag{9}$$

Step 2 Employing (5) and (6) to (9), it gives

$$\begin{cases} \dot{\boldsymbol{\xi}}_x = \boldsymbol{\xi}_v \\ \dot{\boldsymbol{\xi}}_v = \boldsymbol{f}(\boldsymbol{\xi}_v) - \alpha([\boldsymbol{L} \otimes \boldsymbol{I}_p]\boldsymbol{\xi}_x + c[\boldsymbol{L} \otimes \boldsymbol{I}_p]\boldsymbol{\xi}_v)^{\gamma} - \\ \quad \beta \int_0^t ([\boldsymbol{L} \otimes \boldsymbol{I}_p]\boldsymbol{\xi}_x + c[\boldsymbol{L} \otimes \boldsymbol{I}_p]\boldsymbol{\xi}_v)\mathrm{d}\tau \end{cases}. \tag{10}$$

Step 3 For system (10), define the following Lyapunov function V:

$$V = V_x + V_v + \boldsymbol{\xi}_x^{\mathrm{T}} \boldsymbol{I}_p \boldsymbol{\xi}_v = \frac{1}{2}\boldsymbol{\xi}^{\mathrm{T}} \begin{bmatrix} \sigma(\boldsymbol{L} \otimes \boldsymbol{I}_p) & \boldsymbol{I}_p \\ \boldsymbol{I}_p & \boldsymbol{I}_p \end{bmatrix} \boldsymbol{\xi} \tag{11}$$

with

$$\begin{cases} V_x = \dfrac{1}{2}\boldsymbol{\xi}_x^{\mathrm{T}} \sigma(\boldsymbol{L} \otimes \boldsymbol{I}_p)\boldsymbol{\xi}_x V_v = \dfrac{1}{2}\boldsymbol{\xi}_v^{\mathrm{T}} \boldsymbol{I}_p \boldsymbol{\xi}_v \\ \boldsymbol{\xi} = [\ \boldsymbol{\xi}_x^{\mathrm{T}} \quad \boldsymbol{\xi}_v^{\mathrm{T}}\ ]^{\mathrm{T}} \in \mathbf{R}^{2p} \end{cases}. \tag{12}$$

It follows that for $\sigma \in \mathbf{R}^+$, the following condition holds:

$$V \geqslant \frac{1}{2}\boldsymbol{\xi}^{\mathrm{T}} \begin{bmatrix} \sigma\lambda_2(\boldsymbol{L}) & 1 \\ 1 & 1 \end{bmatrix} \otimes \boldsymbol{I}_{n \times p}\boldsymbol{\xi}. \tag{13}$$

Putting (13) under the following form:

$$V \geqslant \frac{1}{2}\boldsymbol{\xi}^{\mathrm{T}} \begin{bmatrix} \boldsymbol{A} & \boldsymbol{B} \\ \boldsymbol{B}^T & \boldsymbol{C} \end{bmatrix} \otimes \boldsymbol{I}_{n \times p}\boldsymbol{\xi} \tag{14}$$

and using Schur 's complement, it follows that if σ is chosen such that $\sigma > 1/\lambda_2(L)$ then V is positive:

$$\boldsymbol{A} - \boldsymbol{B}\boldsymbol{C}^{-1}\boldsymbol{B}^{\mathrm{T}} = \sigma\lambda_2(\boldsymbol{L}) - 1 > 0. \tag{15}$$

Step 4 Next, take the time derivative of the function V along the trajectories (10):

$$\begin{aligned} \dot{V} &= \boldsymbol{\xi}^{\mathrm{T}} \begin{bmatrix} \sigma(\boldsymbol{L} \otimes \boldsymbol{I}_p) & \boldsymbol{I}_p \\ \boldsymbol{I}_p & \boldsymbol{I}_p \end{bmatrix} \dot{\boldsymbol{\xi}} = \\ &\sigma\boldsymbol{\xi}_x^{\mathrm{T}}(\boldsymbol{L} \otimes \boldsymbol{I}_p)\boldsymbol{\xi}_v + \boldsymbol{\xi}_v^{\mathrm{T}}\boldsymbol{I}_p\boldsymbol{\xi}_v + \boldsymbol{\xi}_x^{\mathrm{T}}\boldsymbol{I}_p\dot{\boldsymbol{\xi}}_v + \boldsymbol{\xi}_v^{\mathrm{T}}\boldsymbol{I}_p\dot{\boldsymbol{\xi}}_v = \\ &\sigma\boldsymbol{\xi}_x^{\mathrm{T}}(\boldsymbol{L} \otimes \boldsymbol{I}_p)\boldsymbol{\xi}_v + \boldsymbol{\xi}_v^{\mathrm{T}}\boldsymbol{I}_p\boldsymbol{\xi}_v + \left(\boldsymbol{\xi}_x^{\mathrm{T}} + \boldsymbol{\xi}_v^{\mathrm{T}}\right)\dot{\boldsymbol{\xi}}_v. \end{aligned} \tag{16}$$

Using the system dynamics (10), it results in

$$\begin{aligned} \dot{V} &= \sigma\boldsymbol{\xi}_x^{\mathrm{T}}(\boldsymbol{L} \otimes \boldsymbol{I}_p)\boldsymbol{\xi}_v + \boldsymbol{\xi}_v^{\mathrm{T}}\boldsymbol{\xi}_v + \left(\boldsymbol{\xi}_x^{\mathrm{T}} + \boldsymbol{\xi}_v^{\mathrm{T}}\right)\boldsymbol{f} - \\ &\alpha\left(\boldsymbol{\xi}_x^{\mathrm{T}} + \boldsymbol{\xi}_v^{\mathrm{T}}\right)[(\boldsymbol{L} \otimes \boldsymbol{I}_p)\boldsymbol{\xi}_x + c(\boldsymbol{L} \otimes \boldsymbol{I}_p)\boldsymbol{\xi}_v]^{\gamma} - \\ &\beta\left(\boldsymbol{\xi}_x^{\mathrm{T}} + \boldsymbol{\xi}_v^{\mathrm{T}}\right)\int_0^t [(\boldsymbol{L} \otimes \boldsymbol{I}_p)\boldsymbol{\xi}_x + c(\boldsymbol{L} \otimes \boldsymbol{I}_p)\boldsymbol{\xi}_v]\mathrm{d}\tau. \end{aligned} \tag{17}$$

Applying Newton 's generalized binomial theorem for the case of the fixed-time graph topology, we obtain that

$$\begin{aligned} \dot{V} &= \sigma\boldsymbol{\xi}_x^{\mathrm{T}}(\boldsymbol{L} \otimes \boldsymbol{I}_p)\boldsymbol{\xi}_v + \boldsymbol{\xi}_v^{\mathrm{T}}\boldsymbol{\xi}_v + \left(\boldsymbol{\xi}_x^{\mathrm{T}} + \boldsymbol{\xi}_v^{\mathrm{T}}\right)\boldsymbol{f} - \\ &\alpha\left(\boldsymbol{\xi}_x^{\mathrm{T}} + \boldsymbol{\xi}_v^{\mathrm{T}}\right)\sum_{k=0}^{p}\left[\begin{pmatrix} \gamma \\ k \end{pmatrix}[(\boldsymbol{L} \otimes \boldsymbol{I}_p)\boldsymbol{\xi}_x]^{\gamma-k}[c(\boldsymbol{L} \otimes \boldsymbol{I}_p)\boldsymbol{\xi}_v]^k\right] - \\ &\beta\left(\boldsymbol{\xi}_x^{\mathrm{T}} + \boldsymbol{\xi}_v^{\mathrm{T}}\right)\left[(\boldsymbol{L} \otimes \boldsymbol{I}_p)\int_0^t \boldsymbol{\xi}_x\mathrm{d}\tau + c(\boldsymbol{L} \otimes \boldsymbol{I}_p)\boldsymbol{\xi}_x\right]. \end{aligned} \tag{18}$$

To prove that the condition $\dot{V} < 0$ holds when $\forall t > t_0$, first, we consider the term:

$$\begin{aligned} &\sigma\boldsymbol{\xi}_x^{\mathrm{T}}(\boldsymbol{L} \otimes \boldsymbol{I}_p)\boldsymbol{\xi}_v - \alpha(\boldsymbol{\xi}_x^{\mathrm{T}} + \boldsymbol{\xi}_v^{\mathrm{T}}) \cdot \\ &\sum_{k=0}^{p}\left[\begin{pmatrix} \gamma \\ k \end{pmatrix}[(\boldsymbol{L} \otimes \boldsymbol{I}_p)\boldsymbol{\xi}_x]^{\gamma-k}[c(\boldsymbol{L} \otimes \boldsymbol{I}_p)\boldsymbol{\xi}_v]^k\right]. \end{aligned}$$

To bound this term, we re-write it as follows:

$$\sigma\boldsymbol{\xi}_x^{\mathrm{T}}(\boldsymbol{L}\otimes\boldsymbol{I}_p)\boldsymbol{\xi}_v-\alpha\left(\boldsymbol{\xi}_x^{\mathrm{T}}+\boldsymbol{\xi}_v^{\mathrm{T}}\right)\sum_{k=0}^{p}\left[\begin{pmatrix}\gamma\\k\end{pmatrix}[(\boldsymbol{L}\otimes\boldsymbol{I}_p)\boldsymbol{\xi}_x]^{\gamma-k}[c(\boldsymbol{L}\otimes\boldsymbol{I}_p)\boldsymbol{\xi}_v]^k\right]=$$

$$\sigma\boldsymbol{\xi}_x^{\mathrm{T}}(\boldsymbol{L}\otimes\boldsymbol{I}_p)\boldsymbol{\xi}_v-\alpha\begin{pmatrix}\gamma\\0\end{pmatrix}(\boldsymbol{\xi}_x^{\gamma})^{\mathrm{T}}(\boldsymbol{L}\otimes\boldsymbol{I}_p)^{\gamma}\boldsymbol{\xi}_v-\alpha\sum_{k=1}^{p}\left[c^k\begin{pmatrix}\gamma\\k\end{pmatrix}\left(\boldsymbol{\xi}_x^{\gamma-k}\right)(\boldsymbol{L}\otimes\boldsymbol{I}_p)^{\gamma}\boldsymbol{\xi}_v^k\right]=$$

$$\boldsymbol{\xi}_x^{\mathrm{T}}(\boldsymbol{L}\otimes\boldsymbol{I}_p)\boldsymbol{\xi}_v\left[\sigma-\alpha\begin{pmatrix}\gamma\\0\end{pmatrix}(\boldsymbol{L}\otimes\boldsymbol{I}_p)^{\gamma-1}\boldsymbol{\xi}_x^{\gamma-1}\right]-\alpha\sum_{k=1}^{p}\left[c^k\begin{pmatrix}\gamma\\k\end{pmatrix}\left(\boldsymbol{\xi}_x^{\gamma-k}\right)(\boldsymbol{L}\otimes\boldsymbol{I}_p)^{\gamma}\boldsymbol{\xi}_v^k\right].\tag{19}$$

Based on the properties of the matrix $\boldsymbol{L}$, (19) is bounded as follows:

$$\sigma\boldsymbol{\xi}_x^{\mathrm{T}}(\boldsymbol{L}\otimes\boldsymbol{I}_p)\boldsymbol{\xi}_v-\alpha\left(\boldsymbol{\xi}_x^{\mathrm{T}}+\boldsymbol{\xi}_v^{\mathrm{T}}\right)\sum_{k=0}^{p}\left[\begin{pmatrix}\gamma\\k\end{pmatrix}[(\boldsymbol{L}\otimes\boldsymbol{I}_p)\boldsymbol{\xi}_x]^{\gamma-k}[c(\boldsymbol{L}\otimes\boldsymbol{I}_p)\boldsymbol{\xi}_v]^k\right]\leqslant$$

$$\boldsymbol{\xi}_x^{\mathrm{T}}(\boldsymbol{L}\otimes\boldsymbol{I}_p)\boldsymbol{\xi}_v\left[\sigma-\alpha\begin{pmatrix}\gamma\\0\end{pmatrix}\lambda_2^{\gamma-1}(\boldsymbol{L})\left\|\boldsymbol{\xi}_x^{\gamma-1}\right\|_2\right]-\alpha\sum_{k=1}^{p}\left[c^k\begin{pmatrix}\gamma\\k\end{pmatrix}\left(\boldsymbol{\xi}_x^{\gamma-k}\right)(\boldsymbol{L}\otimes\boldsymbol{I}_p)^{\gamma}\boldsymbol{\xi}_v^k\right].\tag{20}$$

Since the form V_x is a quadratic function of $\|\xi_x\|$, we obtain that

$$\boldsymbol{\xi}_x^{\mathrm{T}}(\boldsymbol{L}\otimes\boldsymbol{I}_p)\boldsymbol{\xi}_v\left[\sigma-\alpha\begin{pmatrix}\gamma\\0\end{pmatrix}\lambda_2^{\gamma-1}(\boldsymbol{L})\left\|\boldsymbol{\xi}_x^{\gamma-1}\right\|_2\right]-$$
$$\alpha\sum_{k=1}^{p}\left[c^k\begin{pmatrix}\gamma\\k\end{pmatrix}\left(\boldsymbol{\xi}_x^{\gamma-k}\right)(\boldsymbol{L}\otimes\boldsymbol{I}_p)^{\gamma}\boldsymbol{\xi}_v^k\right]\leqslant$$
$$\boldsymbol{\xi}_x^{\mathrm{T}}(\boldsymbol{L}\otimes\boldsymbol{I}_p)\boldsymbol{\xi}_v\left[\sigma-\alpha\begin{pmatrix}\gamma\\0\end{pmatrix}\lambda_2^{\gamma-1}(\boldsymbol{L})\left(\frac{2V_x(0)}{\lambda_{\max}(\boldsymbol{L})}\right)^{\gamma-1}\right]-$$
$$\alpha\sum_{k=1}^{p}\left[c^k\begin{pmatrix}\gamma\\k\end{pmatrix}\left(\boldsymbol{\xi}_x^{\gamma-k}\right)(\boldsymbol{L}\otimes\boldsymbol{I}_p)^{\gamma}\boldsymbol{\xi}_v^k\right].\tag{21}$$

Selecting σ as

$$\sigma=\alpha\begin{pmatrix}\gamma\\0\end{pmatrix}\lambda_2^{\gamma}(\boldsymbol{L})\left(\frac{2V_x(0)}{\lambda_{max}(\boldsymbol{L})}\right)^{\gamma-1}>\frac{1}{\lambda_2(\boldsymbol{L})},\tag{22}$$

the control gain α can be set as

$$\alpha>\begin{pmatrix}\gamma\\0\end{pmatrix}^{-1}\frac{1}{\lambda_2^{\gamma+1}(\boldsymbol{L})}\left(\frac{2V_x(0)}{\lambda_{max}(\boldsymbol{L})}\right)^{1-\gamma}.\tag{23}$$

Employing condition (23) to (21) yields

$$\sigma\boldsymbol{\xi}_x^{\mathrm{T}}(\boldsymbol{L}\otimes\boldsymbol{I}_p)\boldsymbol{\xi}_v-\alpha\sum_{k=0}^{p}\left[\begin{pmatrix}\gamma\\k\end{pmatrix}[(\boldsymbol{L}\otimes\boldsymbol{I}_p)\boldsymbol{\xi}_x]^{\gamma-k}[c(\boldsymbol{L}\otimes\boldsymbol{I}_p)\boldsymbol{\xi}_v]^k\right]\leqslant-\alpha\sum_{k=1}^{p}\left[c^k\begin{pmatrix}\gamma\\k\end{pmatrix}\left(\boldsymbol{\xi}_x^{\gamma-k}\right)(\boldsymbol{L}\otimes\boldsymbol{I}_p)^{\gamma}\boldsymbol{\xi}_v^k\right].\tag{24}$$

Second, the integral term in (17) $\beta(\boldsymbol{\xi}_x^{\mathrm{T}}+\boldsymbol{\xi}_v^{\mathrm{T}})(1+c)(\boldsymbol{L}\otimes\boldsymbol{I}_p)\int_0^t\boldsymbol{\xi}_x\mathrm{d}\tau$ can be bounded by considering Cauchy-Schwarz inequality:

$$\beta\left(\boldsymbol{\xi}_x^{\mathrm{T}}+\boldsymbol{\xi}_v^{\mathrm{T}}\right)(\boldsymbol{L}\otimes\boldsymbol{I}_p)\int_0^t\boldsymbol{\xi}_x\mathrm{d}\tau\leqslant$$
$$\beta(\boldsymbol{L}\otimes\boldsymbol{I}_p)\int_0^t\left[\left(\boldsymbol{\xi}_x^{\mathrm{T}}+\boldsymbol{\xi}_v^{\mathrm{T}}\right)\boldsymbol{\xi}_x\right]\mathrm{d}\tau\leqslant$$
$$\beta(\boldsymbol{L}\otimes\boldsymbol{I}_p)\int_0^t\left(\left\|\boldsymbol{\xi}_x^{\mathrm{T}}\right\|_2\|\boldsymbol{\xi}_x\|_2+\left\|\boldsymbol{\xi}_v^{\mathrm{T}}\right\|_2\|\boldsymbol{\xi}_x\|_2\right)\mathrm{d}\tau\leqslant$$
$$\beta\lambda_{\max}(\boldsymbol{L}\otimes\boldsymbol{I}_p)\left(\|\boldsymbol{\xi}_x\|_2^2+\left\|\boldsymbol{\xi}_v^{\mathrm{T}}\right\|_2\|\boldsymbol{\xi}_x\|_2\right).\tag{25}$$

From (24) and (25), it results in that

$$\dot{V}\leqslant\boldsymbol{\xi}_v^{\mathrm{T}}\boldsymbol{\xi}_v+\alpha\left\|\boldsymbol{\xi}_x^{\mathrm{T}}+\boldsymbol{\xi}_v^{\mathrm{T}}\right\|_2\delta_{f_i}-$$
$$\alpha\boldsymbol{\xi}_v^{\mathrm{T}}\sum_{k=1}^{p}\left[c^k\begin{pmatrix}\gamma\\k\end{pmatrix}\left(\boldsymbol{\xi}_x^{\gamma-k}\right)(\boldsymbol{L}\otimes\boldsymbol{I}_p)^{\gamma}\boldsymbol{\xi}_v^k\right]-$$
$$\beta(1+c)\lambda_{\max}(\boldsymbol{L}\otimes\boldsymbol{I}_p)\left(\|\boldsymbol{\xi}_x\|_2^2+\left\|\boldsymbol{\xi}_v^{\mathrm{T}}\right\|_2\|\boldsymbol{\xi}_x\|_2\right).\tag{26}$$

In order to find the necessary conditions for $\dot{V}<0$, $\forall t>t_0$, (26) is arranged as follows:

$$\dot{V}\leqslant-\alpha\boldsymbol{\xi}_v^{\mathrm{T}}\sum_{k=1}^{p}\left[c^k\begin{pmatrix}\gamma\\k\end{pmatrix}\left(\boldsymbol{\xi}_x^{\gamma-k}\right)(\boldsymbol{L}\otimes\boldsymbol{I}_p)^{\gamma}\boldsymbol{\xi}_v^k\right]+\boldsymbol{\xi}^{\mathrm{T}}\boldsymbol{Q}\boldsymbol{\xi}\tag{27}$$

where

$$\begin{cases}Q_{11}=(1+\alpha\delta_{f_i})\\Q_{12}=Q_{21}=\dfrac{1}{2}\beta(1+c)\lambda_{\max}(\boldsymbol{L}\otimes\boldsymbol{I}_p)\\Q_{22}=\dfrac{1}{2}\beta(1+c)\lambda_{\max}(\boldsymbol{L}\otimes\boldsymbol{I}_p)\end{cases}.\tag{28}$$

From (27), it can be seen that $\dot{V}$ is negatively definite if

$$\alpha\delta_{f_i}-\beta(1+c)\lambda_{\max}(\boldsymbol{L}\otimes\boldsymbol{I}_p)<0\tag{29}$$

which results in

$$\beta>\frac{\alpha\delta_{f_i}}{(1+c)\lambda_{\max}(\boldsymbol{L}\otimes\boldsymbol{I}_p)}.\tag{30}$$

4. Distributed cooperative control for UAV MAS

4.1 UAV MAS dynamics

Consider a multi-vehicle autonomous system of n UAVs and suppose that the three-dimensional trajectory of each vehicle $i \in \mathcal{N}$ is described by a vector $\boldsymbol{q}_i$ such that

$$\begin{aligned}\boldsymbol{q}_i &= [\ \boldsymbol{x}_i,\quad \boldsymbol{\vartheta}_i\ ]^{\mathrm{T}} = \\ &[\ \langle x_i, y_i, z_i\rangle^{\mathrm{T}},\quad \langle \gamma_i, \theta_i, \psi_i\rangle^{\mathrm{T}}\ ]^{\mathrm{T}} \in \mathbf{R}^6\end{aligned} \tag{31}$$

where $\boldsymbol{x}_i$ is the position vector and $\boldsymbol{\vartheta}_i$ is the angular rotation vector, i.e., roll, pitch, and yaw, as shown in Fig. 1 [23].

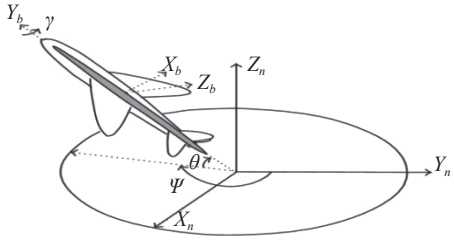

Fig. 1 UAV motion in 3D space: inertial frame, body frame, and Euler angles

The angular velocity vector $\boldsymbol{\omega}_i$ is given, in the body airframe, by

$$\boldsymbol{\omega}_i = \begin{bmatrix} 1 & 0 & -\sin\theta \\ 0 & \cos\gamma & \cos\theta\sin\gamma \\ 0 & \sin\gamma & \cos\theta\cos\gamma \end{bmatrix} \dot{\boldsymbol{\vartheta}}_i. \tag{32}$$

According to the frame configuration shown in Fig. 1, we consider the following dynamic models for both agents and leader.

Agents:

$$\begin{cases} \dot{\boldsymbol{x}}_i = \boldsymbol{v}_i, \quad \dot{\boldsymbol{v}}_i = \boldsymbol{f}_{it} + \boldsymbol{u}_{it} \\ \dot{\vartheta}_i = \omega_i, \quad \dot{\omega}_i = \boldsymbol{f}_{ir} + \boldsymbol{u}_{ir} \end{cases} \tag{33}$$

Leader:

$$\begin{cases} \dot{\boldsymbol{x}}_0 = \boldsymbol{v}_0, \quad \dot{\boldsymbol{v}}_0 = \boldsymbol{f}_{t0} \\ \dot{\vartheta}_0 = \boldsymbol{T}^{-1}\omega_0, \quad \dot{\omega}_0 = \boldsymbol{f}_{r0} \end{cases} \tag{34}$$

where the subscripts t and r denote translational and rotational motions, respectively; $f_{it} = T^{-1} f_{t0}$, $f_{it} = f_{r0}$; T is the matrix that relates the body frame to the inertial frame and it is given, from Euler rotations, as

$$\boldsymbol{T} = \begin{bmatrix} \cos\gamma\cos\psi - \cos\theta\sin\gamma\sin\psi & -\cos\psi\sin\gamma - \cos\gamma\cos\theta\sin\psi & \sin\theta\sin\psi \\ \cos\theta\cos\psi\sin\gamma - \cos\gamma\sin\psi & \cos\gamma\cos\theta\cos\psi - \sin\gamma\sin\psi & -\cos\psi\sin\theta \\ \sin\gamma\sin\theta & \cos\gamma\sin\theta & \cos\theta \end{bmatrix}. \tag{35}$$

4.2 UAV MAS consensus control

Lemma 2 The translational and rotational control inputs $\boldsymbol{u}_{it}$ and $\boldsymbol{u}_{ir}$ are designed according to Theorem 1.

$$\begin{cases} \boldsymbol{u}_{it}(t) = -\alpha_t \boldsymbol{\eta}_{it}^{\gamma} - \beta_t \int_0^t \boldsymbol{\eta}_{it}(\tau)\mathrm{d}\tau \\ \boldsymbol{u}_{ir}(t) = -\alpha_r \boldsymbol{\eta}_{ir}^{\gamma} - \beta_r \int_0^t \boldsymbol{\eta}_{ir}(\tau)\mathrm{d}\tau \end{cases} \tag{36}$$

where α_t, β_t, α_r, and β_r are computed by using (23) and (30), and

$$\begin{cases} \boldsymbol{\eta}_{it}(t) = \sum_{j=0}^{n} a_{ij}(\boldsymbol{x}_i(t) - \boldsymbol{x}_j(t)) + \\ \qquad c\sum_{j=0}^{n} a_{ij}(\boldsymbol{v}_i(t) - \boldsymbol{v}_j(t)) \\ \boldsymbol{\eta}_{ir}(t) = \sum_{j=0}^{n} a_{ij}(\boldsymbol{\vartheta}_i(t) - \boldsymbol{\vartheta}_j(t)) + \\ \qquad c\sum_{j=0}^{n} a_{ij}(\boldsymbol{\omega}_i(t) - \boldsymbol{\omega}_j(t)) \end{cases}. \tag{37}$$

4.3 UAV MAS formation control

The formation control objective is to design translational and rotational controls that enable multi-UAV systems to achieve precise tracking of the desired geometric pattern $\mathcal{P}(x, y, z)$ in three-dimensional space with

$$\sum_{i=1}^{n} p_{ix} = p_{0x}, \quad \sum_{i=1}^{n} p_{iy} = p_{0y}, \quad \sum_{i=1}^{n} p_{iz} = p_{0z} \tag{38}$$

where (p_{x0}, p_{y0}, p_{z0}) is the center of the geometric pattern $\mathcal{P}(x, y, z)$.

Suppose that ζ_{1i}, ζ_{2i}, ζ_{3i} are the formation states, u_{1i}, u_{2i} are the formation control protocols, and the formation evolves according to the following dynamics system [21]:

$$\begin{cases} \dot{\zeta}_{1i} = u_{1i} \\ \dot{\zeta}_{2i} = u_{2i} \\ \dot{\zeta}_{3i} = u_{1i}\zeta_{2i} - k_0 |u_{1i}| \zeta_{3i} \end{cases} \tag{39}$$

where $k_0 \in \mathbf{R}^+$. The agents' trajectories are related to the pattern trajectory as follows:

$$\begin{cases} x_i = \cos(\zeta_{1i})[\zeta_{2i} - k_0 \mathrm{sign}(u_{1i})\zeta_{3i}] + \\ \qquad \sin(\zeta_{1i})\zeta_{3i} + p_{xi} \\ y_i = \sin(\zeta_{1i})[\zeta_{2i} - k_0 \mathrm{sign}(u_{1i})\zeta_{3i}] - \\ \qquad \cos(\zeta_{1i})\zeta_{3i} + p_{yi} \\ z_i = p_{zi} \end{cases}. \tag{40}$$

If $\lim_{t\to\infty}(\zeta_{ki} - \zeta_{k0}) = 0$ and $\lim_{t\to\infty}(u_{li} - u_{l0}) = 0$ for $k = 1, 2, 3$; $l = 1, 2$; $1 \leqslant i \leqslant n$, then for $1 \leqslant i \neq j \leqslant n$ the MAS of n-UAV achieves

$$\lim_{t\to\infty}\begin{bmatrix} x_i-x_j \\ y_i-y_j \\ z_i-z_j \end{bmatrix}=\begin{bmatrix} p_{xi}-p_{xj} \\ p_{yi}-p_{yj} \\ p_{zi}-p_{zj} \end{bmatrix},\ \lim_{t\to\infty}\left(\sum_{i=1}^{n}\frac{x_i}{n}-x_0\right)=0,$$
$$\lim_{t\to\infty}\left(\sum_{i=1}^{n}\frac{y_i}{n}-y_0\right)=0,\ \lim_{t\to\infty}\left(\sum_{i=1}^{n}\frac{z_i}{n}-z_0\right)=0 \tag{41}$$

where x_0, y_0, z_0 denote the leader coordinates (the formation pattern centroid). Defining the vector $\tilde{\zeta}_i=[(\zeta_{1i}-\zeta_{10}),(\zeta_{2i}-\zeta_{20}),(\zeta_{3i}-\zeta_{30})]^{\mathrm{T}}$ as the tracking error vector for each UAV i and using the control law (5) for both u_{1i} and u_{2i}, we obtain that

$$\begin{cases} u_{ki}=-\alpha_k\eta_{ki}{}^{\gamma}-\beta_k\int_0^t\eta_{ki}(\tau)\mathrm{d}\tau \\ \eta_{ki}(t)=\sum_{j=0}^{n}a_{ij}(\zeta_{ki}(t)-\zeta_{kj}(t)) \end{cases},\ k=1,2. \tag{42}$$

Substitution of protocols (42) into the first two dynamic equations of system (39) results in the following reduced dynamic system:

$$\begin{cases} \dot{\tilde{\zeta}}_{1i}=-\alpha_1\left(\sum_{j=0}^{n}a_{ij}(\zeta_{1i}(t)-\zeta_{1j}(t))\right)_i^{\gamma}- \\ \qquad\beta_1\int_0^t\left(\sum_{j=0}^{n}a_{ij}(\zeta_{1i}(\tau)-\zeta_{1j}(\tau))\right)\mathrm{d}\tau+\dot{\zeta}_{10} \\ \dot{\tilde{\zeta}}_{2i}=-\alpha_2\left(\sum_{j=0}^{n}a_{ij}(\zeta_{2i}(t)-\zeta_{2j}(t))\right)- \\ \qquad\beta_2\int_0^t\left(\sum_{j=0}^{n}a_{ij}(\zeta_{2i}(\tau)-\zeta_{2j}(\tau))\right)\mathrm{d}\tau+\dot{\zeta}_{20} \end{cases}. \tag{43}$$

Equation (43) is equivalent, in a vector form, to the following auxiliary closed-loop system:

$$\dot{\tilde{\zeta}}=-\alpha\left[(\boldsymbol{L}\otimes\boldsymbol{I}_2)\tilde{\zeta}\right]^{\gamma}-\beta\int_0^t\left[(\boldsymbol{L}\otimes\boldsymbol{I}_2)\tilde{\zeta}(\tau)\right]\mathrm{d}\tau-\dot{\zeta}_0 \tag{44}$$

where

$$\tilde{\boldsymbol{\zeta}}=\begin{bmatrix}\tilde{\zeta}_1^{\mathrm{T}}, & \tilde{\zeta}_2^{\mathrm{T}}\end{bmatrix}^{\mathrm{T}}=[\ \tilde{\zeta}_{11},\cdots,\tilde{\zeta}_{1n},\ \ \tilde{\zeta}_{21},\cdots,\tilde{\zeta}_{2n}\ ]^{\mathrm{T}}$$

$$\tilde{\boldsymbol{\zeta}}_0=\begin{bmatrix}\mathbf{1}_n^{\mathrm{T}}\tilde{\zeta}_{10}, & \mathbf{1}_n^{\mathrm{T}}\tilde{\zeta}_{20}\end{bmatrix}^{\mathrm{T}}$$

$$\boldsymbol{\alpha}=\begin{bmatrix}\alpha_1\boldsymbol{I}_n & \mathbf{0}_{nn}\\ \mathbf{0}_{nn} & \alpha_2\boldsymbol{I}_n\end{bmatrix},\ \boldsymbol{\beta}=\begin{bmatrix}\beta_1\boldsymbol{I}_n & \mathbf{0}_{nn}\\ \mathbf{0}_{nn} & \beta_2\boldsymbol{I}_n\end{bmatrix}.$$

Theorem 2 Suppose that the communication graph $\mathcal{G}$ is connected, Assumptions 1−3 are satisfied, and the control inputs to the closed-loop system (45) are chosen by (42), if the tracking error converges to zero, $\lim_{t\to\infty}(\tilde{\zeta}_i)=0$, then the agents' states ζ_{1i} and ζ_{2i} converge to the formation states ζ_{10} and ζ_{20}, respectively.

Proof Consider the following quadratic function as a Lyapunov function candidate

$$V=\frac{1}{2}\tilde{\zeta}^{\mathrm{T}}(\boldsymbol{L}\otimes\boldsymbol{I}_2)\tilde{\zeta} \tag{45}$$

and suppose that the function V is continuously differentiable with respect to $\boldsymbol{\zeta}$, the time-derivative of V is given as

$$\dot{V}=\tilde{\zeta}^{\mathrm{T}}(\boldsymbol{L}\otimes\boldsymbol{I}_2)\dot{\tilde{\zeta}}. \tag{46}$$

Using the auxiliary closed-loop system (44), we obtain

$$\dot{V}=-\alpha\tilde{\zeta}^{\mathrm{T}}(\boldsymbol{L}\otimes\boldsymbol{I}_2)\left[(\boldsymbol{L}\otimes\boldsymbol{I}_2)\tilde{\zeta}\right]^{\gamma}-$$
$$\tilde{\zeta}^{\mathrm{T}}(\boldsymbol{L}\otimes\boldsymbol{I}_2)\beta\int_0^t\left[(\boldsymbol{L}\otimes\boldsymbol{I}_2)\tilde{\zeta}(\tau)\right]\mathrm{d}\tau-\dot{\zeta}_0. \tag{47}$$

As $\gamma>0$ and the gain matrices $\boldsymbol{\alpha}$ and $\boldsymbol{\beta}$ are diagonal, it follows that

$$\dot{V}\leqslant-\det(\boldsymbol{\alpha})\tilde{\zeta}^{\mathrm{T}}(\boldsymbol{L}\otimes\boldsymbol{I}_2)\left[(\boldsymbol{L}\otimes\boldsymbol{I}_2)\tilde{\zeta}\right]^{\gamma}-$$
$$\det(\boldsymbol{\beta})\tilde{\zeta}^{\mathrm{T}}(\boldsymbol{L}\otimes\boldsymbol{I}_2)^2\tilde{\zeta}. \tag{48}$$

Inequation (48) also satisfies

$$\dot{V}\leqslant-\det(\boldsymbol{\beta})\lambda_{\min}^2(\boldsymbol{L}\otimes\boldsymbol{I}_2)\left\|\tilde{\zeta}\right\|_2^2. \tag{49}$$

Since $V=\frac{1}{2}\tilde{\zeta}^{\mathrm{T}}(\boldsymbol{L}\otimes\boldsymbol{I}_2)\tilde{\zeta}\leqslant\frac{1}{2}\lambda_{\max}(\boldsymbol{L}\otimes\boldsymbol{I}_2)\left\|\tilde{\zeta}\right\|_2^2$ and $\lambda_i(\boldsymbol{L}\otimes\boldsymbol{I}_2)=\lambda_i(\boldsymbol{L})$, it follows that

$$\dot{V}\leqslant-\det(\boldsymbol{\beta})\frac{\sqrt{2}\lambda_{\min}^2(\boldsymbol{L})}{\sqrt{\lambda_{\max}(\boldsymbol{L})}}\sqrt{V}. \tag{50}$$

From (50), it can be found that

$$\sqrt{V}\leqslant\sqrt{V_0}-\frac{\det(\boldsymbol{\beta})}{\sqrt{2}}\frac{\lambda_{\min}^2(\boldsymbol{L})}{\sqrt{\lambda_{\max}(\boldsymbol{L})}}t. \tag{51}$$

Let $\sqrt{V}=0$, the convergence of the formation tracking is guaranteed for

$$t\geqslant\sqrt{V_0}\frac{\sqrt{2}}{\det(\boldsymbol{\beta})}\frac{\sqrt{\lambda_{\max}(\boldsymbol{L})}}{\lambda_{\min}^2(\boldsymbol{L})}=$$
$$\frac{\sqrt{\tilde{\zeta}^{\mathrm{T}}(0)(\boldsymbol{L}\otimes\boldsymbol{I}_2)\tilde{\zeta}(0)}}{\det(\boldsymbol{\beta})}\frac{\sqrt{\lambda_{\max}(\boldsymbol{L})}}{\lambda_{\min}^2(\boldsymbol{L})}. \tag{52}$$

□

5. Simulation

5.1 Aerobatic consensus

In this simulation scenario, a group of $n=4$ UAVs perform a path following mission. The considered path is a repeated aerobatic maneuvering in air where the parametric trajectory is defined as follows:

$$\begin{cases} x_0=r\cos^2t+\delta_x \\ y_0=r\cos t\sin t \\ z_0=ar\sin t \end{cases} \tag{53}$$

with r being the radius of the path, $\delta_x=(Nc-1)$ and Nc

being the number of cycles. The leader's initial position is $\boldsymbol{x}_0 = [100, 0, 300]^{\mathrm{T}}$ m with $r = 15$ m, a=10, $Nc = 8$, and $t = [0, 2\pi]$. The agents start the consensus from identical initial speed $\boldsymbol{v}_0 = [25, 0, 0]$ m/s and different initial positions $\boldsymbol{x}_{10} = [100, 75, 200]$ m, $\boldsymbol{x}_{20} = [100, 10, 600]$ m, $\boldsymbol{x}_{30} = [100, 50, 200]$ m, $\boldsymbol{x}_{40} = [100, 25, 400]$ m. The initial agents' orientations are randomly selected as $\boldsymbol{\varphi}_0 = (30°, -45°, 45°, 120°)$, $\boldsymbol{\theta}_0 = (60°, 30°, -60°, -30°)$, and $\boldsymbol{\psi}_0 = (120°, 60°, -120°, -60°)$. The multi-UAV system tracks the common 3D trajectory (52) in repeated cycles under the mixed switching topology shown in Fig. 2 where agents partially loose the communication with the leader. The triplet (α, β, γ) in controller (5) is selected for translation motion as $(1.5, 0.5, 0.85)$ and for rotational motion as $(2, 0.1, 0.85)$.

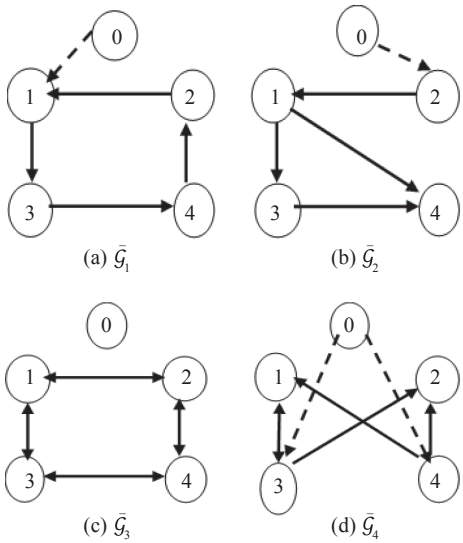

Fig. 2 Fixed-time switching topology connected interaction graph

Fig. 3 shows the three-dimensional consensus of the group of four agents from different angles of view, and Fig. 4 depicts the time history of the convergence of agents' orientations to those corresponding to the virtual leader.

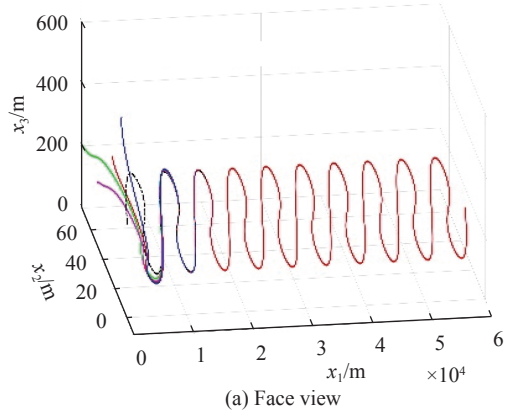

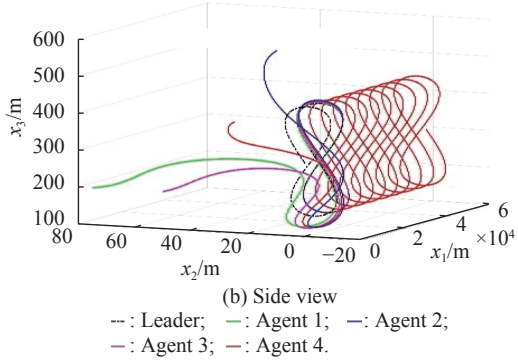

Fig. 3 Cyclic path following from different angles of view

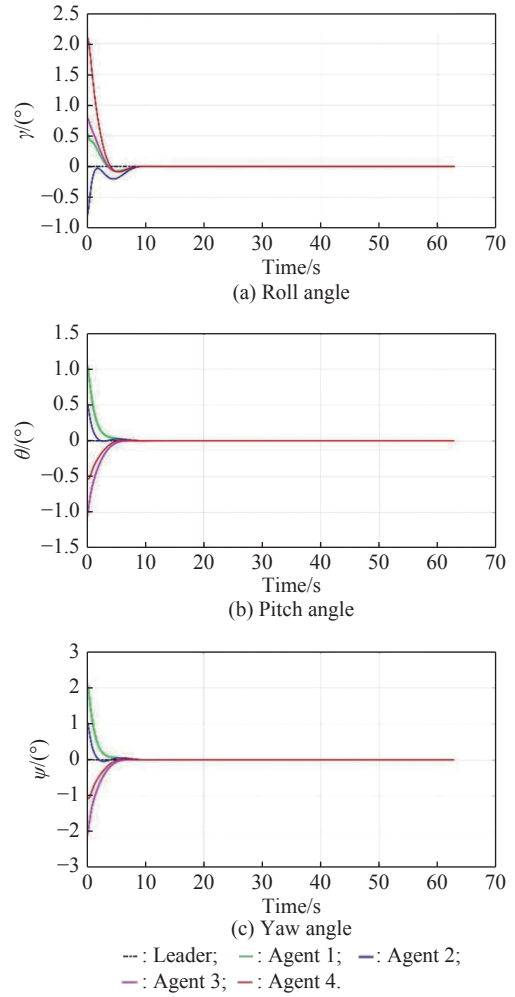

Fig. 4 Time history of agents' orientations

5.2 Tracking of helicoidal formation pattern

In this simulation, we consider a group of $n = 6$ autonomous UAVs performing a desired geometric pattern in space. The center of the formation maintains the geometric pattern along a three-dimensional helical path or helix as shown in Fig. 5(a). On ground, i.e., plane (x, y), the pattern is given by the orthogonal coordinates $(p_{1x},$

$p_{1y}) = (r,0)$, $(p_{2x}, p_{2y}) = \left(\frac{r}{2}, \frac{r}{2}\sqrt{3}\right)$,$(p_{3x}, p_{3y}) = \left(-\frac{r}{2}, \frac{r}{2}\sqrt{3}\right)$, $(p_{4x}, p_{4y}) = (-r,0)$, $(p_{5x}, p_{5y}) = \left(-\frac{r}{2}, \frac{r}{2}\sqrt{3}\right)$ and $(p_{6x}, p_{6y}) = \left(\frac{r}{2}, -\frac{r}{2}\sqrt{3}\right)$, where $r = 6$ m is the hexagon radius. The reference helical trajectory shown in Fig. 5(b) is performed by the pattern centroid and is chosen as $(x_0, y_0, z_0) = \left(R\sin\left(\frac{t}{2}\right), -R\cos\left(\frac{t}{2}\right), h_0 + v_0 t\right)$ where $R = 15$ m is the helix radius, $v_0 = 13.88$ m/s(50 km/h) is the climb rate, and $h_0 = 200$ m is the initial altitude. The formation mission is accomplished under the switching communication topology shown in Fig. 6 with a dwell time of 15 s. The triplet (α, β, γ) in controller (5) is selected as $(5, 1.5, 0.75)$ for both translational and rotational motions.

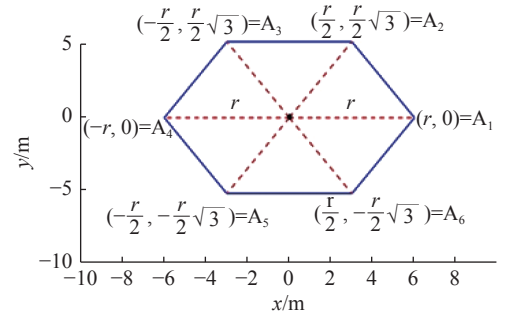

(a) Geometric pattern

(b) Pattern centroid trajectory

Fig. 5 Desired flying formation

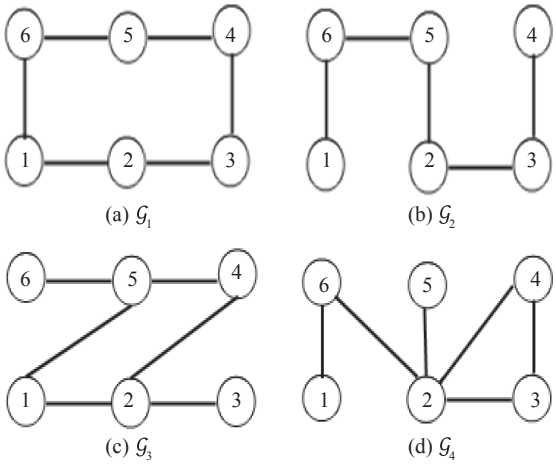

(a) $\mathcal{G}_1$ (b) $\mathcal{G}_2$

(c) $\mathcal{G}_3$ (d) $\mathcal{G}_4$

Fig. 6 Fixed-time switching topology interaction graph

The effectiveness of the proposed control law is validated and compared to the protocol integral sliding mode (ISM) obtained by [24]. In this scenario, the control law (42) is run with $\gamma = 0.75$, $\alpha_1 = 5$, $\beta_1 = 1.5$, $\alpha_2 = \beta_2 = 0$, and the ISM protocol in [24] is run with $\alpha_1 = 0.5, \alpha_2 = 0.67$, and $k_1 = k_2 = 0.25$. Fig. 7 shows the formation tracking using the protocol (42), while Fig. 8 depicts the centroid formation trajectory along the motion axes for both controllers (42) and ISM. The corresponding control inputs are illustrated in Fig. 9.

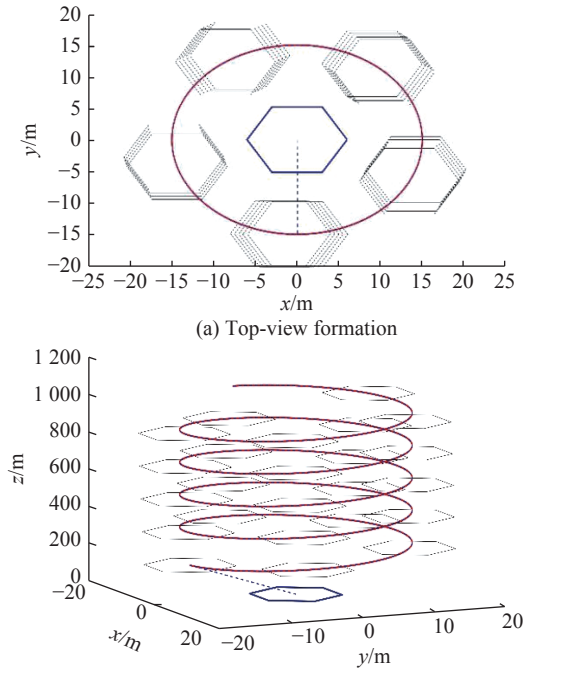

(a) Top-view formation

(b) 3D view formation

Fig. 7 Formation tracking with the control law (42)

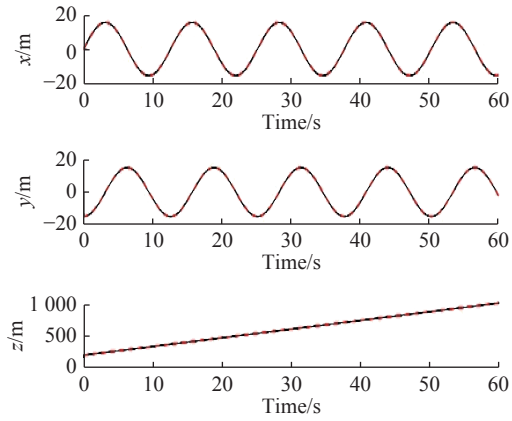

(a) Control law (42)

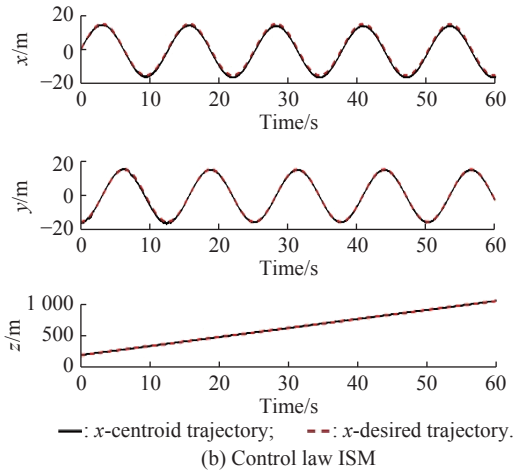

(b) Control law ISM

Fig. 8 Geometric pattern centroid tracking

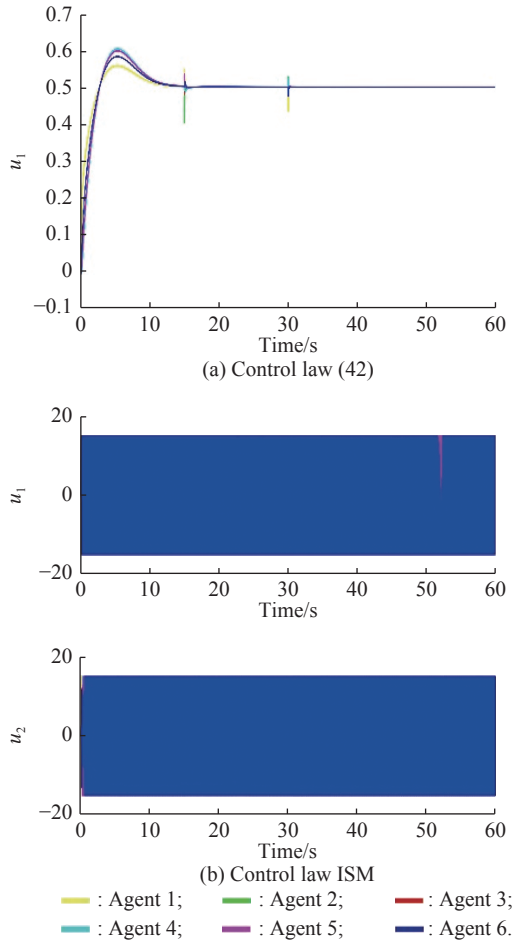

(a) Control law (42)

(b) Control law ISM

Fig. 9 Control inputs (protocols)

5.3 Formation control under undirected topology graph

Consider the case of formation flying of three agents where the communication topology among these agents is described by the undirected graph shown in Fig. 10 [25].

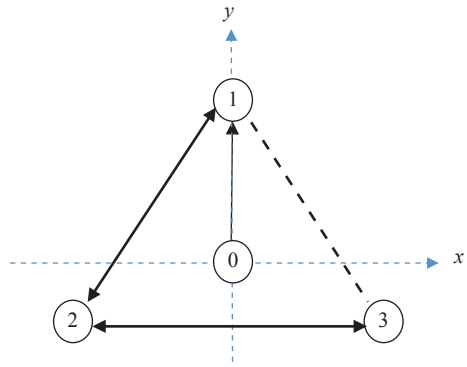

Fig. 10 Triangular formation under undirected communication topology

The triangular pattern is given by $(p_{1x}, p_{1y}) = (0, 2)$, $(p_{2x}, p_{2y}) = (-2, -1)$, and $(p_{3x}, p_{3y}) = (2, -1)$. The leader path is a parametrical trajectory $(x_0, y_0, z_0) = (5\sin 0.2t, -5\cos 0.2t, 0.5t)$. The triplet (α, β, γ) in controller (5) is selected as $(2.5, 2.75, 0.5)$ for translation and $(1.15, 0.25, 0.5)$ for rotation. Fig. 11 shows the agents' trajectories while Fig. 12 depicts the control inputs of the formation model (39). The results below demonstrate the effectiveness and competitiveness of the proposed control strategy as compared to the one presented in [25].

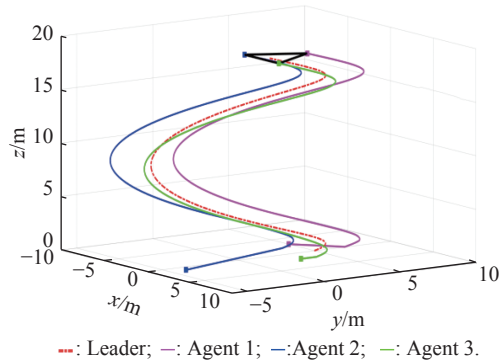

Fig. 11 Formation tracking of triangular pattern

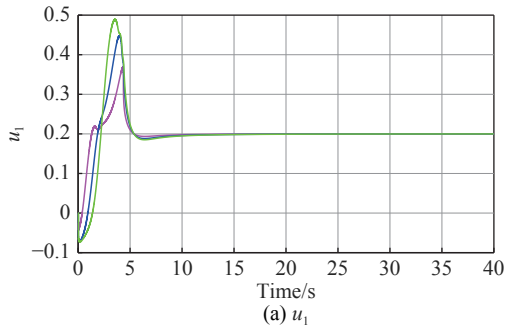

(a) u_1

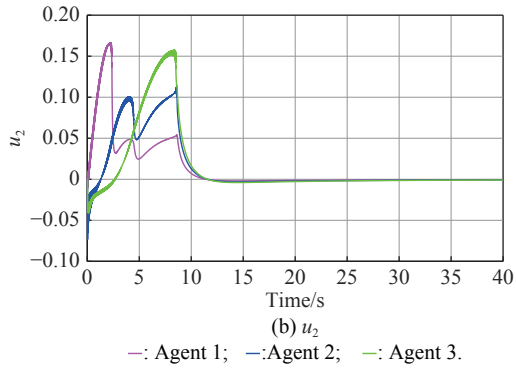

Fig. 12 Control effort

6. Conclusions

In this paper, a smooth distributed cooperative control for multiple flying vehicles such as UAVs is developed based on the concept of the leader-following consensus of MAS. First, in contrast to the conventional sliding-mode based consensus, a smooth distributed consensus algorithm is developed by using proportional and integral continuous functions instead of the discontinuous signum function. Second, a formation control model for three-dimensional geometric pattern tracking is designed. The flying formation scheme employs transitional and rotational smooth control inputs into a three-dimensional motion formation dynamic model. Using the Lyapunov function approach, sufficient conditions are established to ensure the convergence of the consensus and formation models. The effectiveness of the proposed models is demonstrated through complex simulation scenarios such as aerobatic maneuvering, switching communication topology, loss of communication with the leader, and formation control through the helicoidal path.

In the future, the focus will be on multi-UAV formation control with hardware-in-the-loop, formation tracking in presence of external disturbance, and obstacle avoidance among flying agents.

References

[1] GIRARDET B, LAPASSET L, DELAHAYE D, et al. Generating optimal aircraft trajectories with respect to weather conditions. Proc. of the 2nd International Conference on Interdisciplinary Science for Innovative Air Traffic Management, 2013: 1−11.

[2] EI A G, ZHANG L Y, DING Q J. Multi-aircraft cooperative fire assignment based on auction algorithm. Journal of Systems Engineering and Electronics, 2012, 34(9): 1829–1833. (in Chinese)

[3] CHEN F. Aircraft taxiing route planning based on multi-agent system. Proc. of the IEEE Advanced Information Management, Communicates, Electronic and Automation Control Conference, 2016. DOI:10.1109/IMCEC.2016.7867448.

[4] KARIMODDINI A, CHEN B M, LEE T H. Hybrid three-dimensional formation control for unmanned helicopters. Automatica, 2013, 49(2): 424–433.

[5] ZHANG J Q, YE D, BIGGS J D, et al. Finite-time relative orbit-attitude tracking control for multi-spacecraft with collision avoidance and changing network topologies. Advances in Space Research, 2019, 63(3): 1161–1175.

[6] GUO Y H, ZHOU J, LIU Y Y. Distributed RISE control for spacecraft formation reconfiguration with collision avoidance. Journal of the Franklin Institute, 2019, 356(10): 5332–5352.

[7] SKOBELEV P O, SIMONOVA E V, ZHILYAEV A A, et al. Application of multi-agent technology in the scheduling system of swarm of earth remote sensing satellites. Procedia Computer Science, 2017, 103: 396–402.

[8] ZHENG Z X, GUO J, GILL E. Distributed onboard mission planning for multi-satellite systems. Aerospace Science and Technology, 2019, 89: 111–122.

[9] LIU X, LIU L, WANG Y J. Minimum time state consensus for cooperative attack of multi-missile systems. Aerospace Science and Technology, 2017, 69: 87–96.

[10] LYU T, GUO Y N, LI C J, et al. Multiple missiles cooperative guidance with simultaneous attack requirement under directed topologies. Aerospace Science and Technology, 2019, 89: 100–110.

[11] LIU YF, ZHANG A. Cooperative task assignment method of manned/unmanned aerial vehicle formation. Journal of Systems Engineering and Electronics, 2010, 32(3):584-587. (in Chinese)

[12] LIN W. Distributed UAV formation control using differential game approach. Aerospace Science and Technology, 2014, 35: 54–62.

[13] DU H B, ZHU W W, WEN G H, et al. Distributed formation control of multiple quadrotor aircraft based on nonsmooth consensus algorithms. IEEE Trans. on Cybernetics, 2017, 49(1): 2168–2267.

[14] LIANG Z, YI L, XU S D, et al. Multiple UAVs cooperative formation forming control based on back-stepping-like approach. Journal of Systems Engineering and Electronics, 2018, 29(4): 816–822.

[15] ZHANG B Y, SUN X X, LIU S G, et al. Adaptive differential evolution based distributed model predictive control for multi-UAV formation flight. International Journal of Aeronautical and Space Science, 2020, 21. https://doi.org/10.1007/s42405-019-00228-8.

[16] DONG X W, HUA Y Z, ZHOU Y, et al. Theory and experiment on formation-containment control of multiple multirotor unmanned aerial vehicle systems. IEEE Trans. on Automation Science and Engineering, 2019, 16(1): 229–240.

[17] ZHEN Z Y, ZHU P, XUE Y X, et al. Distributed intelligent self-organized mission planning of multi-UAV for dynamic targets cooperative search-attack. Chinese Journal of Aeronautics, 2019, 32(12): 2706–2716.

[18] HU J W, WANG M, ZHAO C H, et al. Formation control and collision avoidance for multi-UAV systems based on Voronoi partition. Science China Technological Sciences, 2020, 63(1): 65–72.

[19] SHAO S K, PENG Y, HE C L, et al. Efficient path planning for UAV formation via comprehensively improved particle swarm optimization. ISA Transactions, 2020, 97: 415–430.

[20] ALMALKI A, KADA B. Consensus tracking for multi-agent systems under bounded unknown external disturbances using sliding-PID control. International Journal of Sciences: Basic and Applied Research, 2020, 50(2): 143–153.

[21] PENG Z X, YANG S C, WEN G G, et al. Adaptive distributed formation control for multiple nonholonomic wheeled mobile robots. Neurocomputing, 2016, 173(3): 1485–1494.
[22] GODSIL C, ROYLE G. Algebraic graph theory (Graduate texts in mathematics). New York: Springer, 2001.
[23] ZHAO L, WANG Q W. Design of an attitude and heading reference system based on distributed filtering for small UAV. Mathematical Problems in Engineering, 2013: 498739.
[24] YU S H, LONG X J. Finite-time consensus for second-order multi-agent systems with disturbances by integral sliding mode. Automatica, 2015, 54: 158–165.
[25] ZHANG X H, GAO J L, ZHANG W F, et al. Distributed formation control for multiple quadrotor based on multi-agent theory and disturbance observer. Mathematical Problems in Engineering, 2019: 7234969.

Biographies

BELKACEM Kada received his B. E. and M. S. degrees from USTO University, Oran, Algeria and Ph. D. degree from Laval University, Quebec, Canada, in 1992, 1998, and 2006, respectively, all in mechanical engineering. From 1993 to 2000, he was a lecturer at the Department of Mechanical Engineering, Mascara University, Algeria. Since 2008, he has been with the Department of Aerospace Engineering, King Abdulaziz University, Saudi Arabia, where he is currently an associate professor, and director of the Aerospace Control Laboratory and the Autonomous Vehicles Center of Research. His current research interests include aerospace control systems, autonomous multi-agent systems, and industrial automation.
E-mail: bkada@kau.edu.sa

MUNAWAR Khalid is a professor of Electrical and Computer Engineering at King Abdulaziz University, Saudi Arabia. He received his B.S. degree in electrical engineering from the University of Engineering and Technology, Lahore, Pakistan in 1992, and M.S. and Ph.D. degrees in aeronautics and space engineering from Tohoku University, Sendai, Japan in 1997 and 2000. He worked as an assistant professor at Tohoku University before moving to the National University of Sciences and Technology, Islamabad, Pakistan in 2002. Then he moved to King Abdulaziz University, Saudi Arabia in 2012. His research interests include control systems, industrial automation, unmanned and autonomous systems, and navigation and control.
E-mail: kmunawar@kau.edu.sa

MUHAMMAD Shafique Shaikh received his B.S. and M.S. degrees in electronics and computer technology from University of Sind, Pakistan, in 1983 and 1984, respectively. He received his M.E. degree in computer science and systems engineering, and D.E. degree in information and production systems engineering, from Muroran Institute of Technology, Hokkaido, Japan, in 1999 and 2002, respectively. Currently, he is working as an assistant professor in Department of Electrical and Computer Engineering, King Abdulaziz University, Saudi Arabia. His research interests include digital signal/image processing, digital image security, neural networks, satellite engineering, and computer and control engineering.
E-mail: msmuhammad@kau.edu.sa